

CLIFF: Continual Learning for Incremental Flake Features in 2D Quantum Material Identification

Sankalp Pandey* Xuan Bac Nguyen Nicholas Borys Hugh Churchill Khoa Luu*

S. Pandey*, Dr. X. B. Nguyen, Prof. K. Luu*
 Quantum AI Lab,
 University of Arkansas, Fayetteville, AR, USA
 Email: sankalp@uark.edu (S.P.); khoaluu@uark.edu (K.L.)
 Prof. N. Borys

Department of Physics and Astronomy,
 University of Utah, Salt Lake City, UT, USA
 Email: nicholas.borys@utah.edu

Prof. H. Churchill
 Department of Physics,
 University of Arkansas, Fayetteville, AR, USA
 Email: hchurch@uark.edu

Keywords: *Computer Vision, Continual Learning, Materials Characterization, Optical Microscopy, Two-Dimensional Materials*

Identifying quantum flakes is crucial for scalable quantum hardware; however, automated layer classification from optical microscopy remains challenging due to substantial appearance shifts across different materials. This paper proposes a new Continual-Learning Framework for Flake Layer Classification (CLIFF). To the best of our knowledge, this work represents the first systematic study of continual learning in two-dimensional (2D) materials. The proposed framework enables the model to distinguish materials and their physical and optical properties by freezing the backbone and base head, which are trained on a reference material. For each new material, it learns a material-specific prompt, embedding, and a delta head. A prompt pool and a cosine-similarity gate modulate features and compute material-specific corrections. Additionally, memory replay with knowledge distillation is incorporated. CLIFF achieves competitive accuracy with significantly lower forgetting than naive fine-tuning and a prompt-based baseline.

1 Introduction

Characterizing the layer counts of two-dimensional (2D) material flakes is crucial for the fabrication of van der Waals heterostructures, which facilitate a range of studies and applications, especially those in quantum mechanics [19, 22, 24]. Due to the inherent randomness in the shape and spatial patterns of the flakes, identification and exploration become challenging. Typically, researchers identify flakes through repeated, manual optical microscopy searches, and the samples must be transferred to an Atomic Force Microscope (AFM) for thickness measurements, which doubles the manual effort and significantly limits the complexity and scalability of heterostructure construction. Deep learning approaches aim to overcome manual bottlenecks in classifying flake layers directly from optical images, as highlighted in Figure 1, but these methods exhibit limited versatility. This work, to the best of our knowledge, presents the first systematic study of continual learning for 2D flake-thickness classification. The evaluation is set up as a material-incremental, continual learning problem, where new materials arrive sequentially.

1.1 The Challenges of Automated Flake Identification

The difficulty in automating the identification of 2D materials is estimating the layer count of a flake from optical microscopy images. Typical optical methods cannot distinguish monolayers, bilayers, and few-layer flakes because they require sub-nanometer resolution. Flakes may appear visually similar in optical images but may differ in thickness (e.g., monolayer and bilayer). Under a regular optical microscope, flakes have faint contrast differences with the substrate (e.g., SiO₂/Si), and the contrast between different flake thicknesses can also be subtle and non-linear. Importantly, the subtle visual characteristics for layer count classification are highly dependent on factors that vary across real-world laboratory

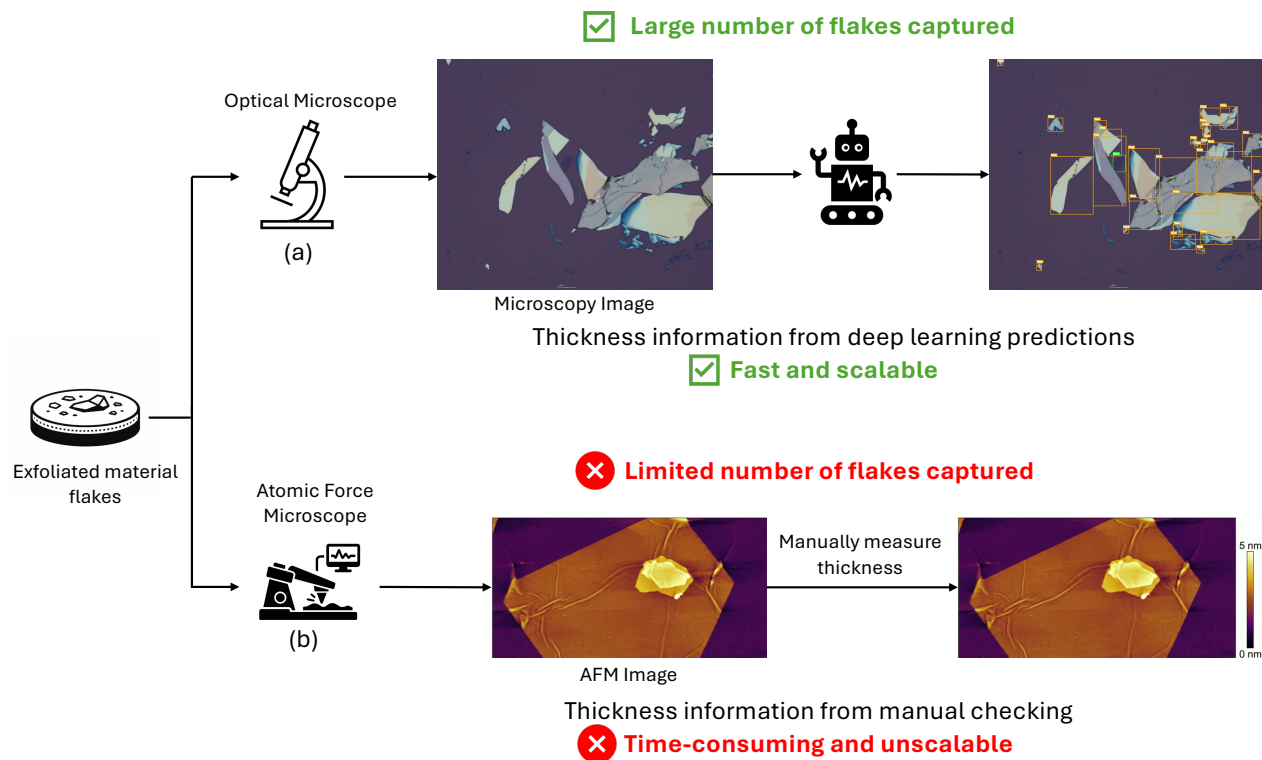


Figure 1: Comparison of 2D material flake characterization methods. **(a)** Automated thickness identification using deep learning on optical microscopy images offers a fast, scalable approach capable of processing large numbers of flakes and predicting their layer count. **(b)** The traditional approach relies on Atomic Force Microscopy (AFM), which is highly accurate but time-consuming and unscalable for high-throughput discovery.

settings. First, different 2D materials, e.g., hBN, graphene, MoS₂, WTe₂, exhibit distinct visual profiles. Second, the appearance of a flake is sensitive to configuration-specific factors, such as illumination conditions and substrate thickness, which may vary between experiments or between datasets. This variability makes it challenging to train a typical deep learning model, motivating the use of a continual learning approach to preserve learned information.

1.2 Limitations of Prior Work

There are critical limitations in traditional and deep learning approaches for flake layer classification from optical microscopy images. Traditional machine learning methods, such as support vector machines (SVMs) [13] and k -nearest neighbors (K-NN) [9], are based on features such as color histograms or texture descriptors, which often fail to represent the subtle and non-linear differences between flakes of different thicknesses. As such, these methods generalize poorly across different imaging setups and materials and are not scalable to large datasets. To address some of these challenges, deep learning approaches [10, 25] aim to learn discriminative features directly from data, but they still have drawbacks. Obtaining a large labeled dataset is difficult, as it requires tools such as AFM or Raman spectroscopy, which pose a fundamental challenge for deep learning models that require large amounts of labeled data. Models tend to overfit to specific materials or imaging conditions and struggle to adapt to new contexts. As previous approaches [54] were developed and evaluated on their own datasets, there are concerns about their applicability in real-world scenarios. When a standard pre-trained model is fine-tuned for a new material or experimental setup, it suffers from catastrophic forgetting, in which performance on the original data degrades severely. This inability of a model to sequentially learn without complete retraining makes it impractical for scientific workflows. To our knowledge, continual learning has not been systematically studied for 2D flake thickness classification, and existing models typically degrade when adapting to new materials.

1.3 Problem Motivation

Addressing these limitations is critical for developing robust automated systems. Although training on a small, fixed set of materials is feasible and can achieve strong performance, it is not a practical strategy for a real-world scientific workflow. In laboratory settings, new materials may be introduced over time, and retraining a large model from scratch with each new dataset can be computationally heavy, especially for larger datasets. Similarly, domain adaptation methods [51, 48, 30, 47, 46, 28, 31, 49] are relevant for handling distribution shifts, but they are typically designed for a single source and target domain. This can be insufficient for a growing sequence of new material domains encountered in a laboratory setting. Therefore, flake layer count classification is formulated as a material-incremental continual learning problem where the model must learn new materials while retaining performance on previously seen materials. To address this, this work proposes a continual learning framework that preserves prior knowledge by freezing a backbone and base head trained on a reference material and learning a per-material addition for each new material.

1.4 Contributions of this Work

This work, to the best of our knowledge, presents the first study on continual learning for 2D material flake thickness classification and the formulation of a material-incremental benchmark. The proposed CLIFF approach is a novel continual learning framework for 2D material flake layer count classification across multiple materials. The evaluation for the CLIFF is conducted under identical splits, metrics, and features, and includes a unified comparison table against joint training, naive fine-tuning, and a popular continual learning approach, Learning-to-Prompt [56].

2 Related Work

2.1 Automatic 2D Materials Thickness Estimation

The exploration of 2D materials has attracted attention in recent years due to their potential to accelerate the development of quantum technologies [7, 33, 29], leading to further advances in quantum algorithms [27, 37, 26, 36] and emerging applications [17, 15, 14, 16]. A deep learning approach using the UNet architecture [43] was used to segment flakes of varying thicknesses. Han et al. [10] were inspired by this method and developed an approach to identify material types from optical microscopy images. They utilized convolutions, batch normalization [18], ReLU activations [1], and a final softmax layer. Masubuchi et al. [25] presented a workflow for 2D flake identification, using Mask R-CNN [12] to predict bounding boxes and segmentation masks for flakes in a given image. Nguyen et al. [32] used self-attention and soft-labeling to identify flake material. Deep learning requires large amounts of training data, so the machine learning paradigm has also been applied, e.g., Gaussian mixture models for flake classification [54]. However, machine learning methods often perform poorly on noisy datasets. In addition, as foundation models grow, zero-shot and few-shot learning are also suitable for 2D material identification [21, 41]. However, learning different materials and setups sequentially requires a continual learning approach to prevent catastrophic forgetting.

2.2 Continual Learning

Continual learning helps prevent catastrophic forgetting in deep learning models. There are several different types of continual learning methods ranging from scene understanding [53, 50, 52] to neuroscience [39, 38]. Rehearsal-based methods store sampled data from previous tasks in buffers [11, 5, 6, 44]. As such, they integrate old and new data to preserve knowledge. Knowledge distillation aims to compress knowledge across older and newer tasks [4, 2, 42, 58]. Self-supervision is also used [40, 3, 34, 35]. Some limitations include buffer size, where making it too small limits learning [3] and restricts access to past data [44]. Some approaches modify the architecture itself, typically by adding new sets of

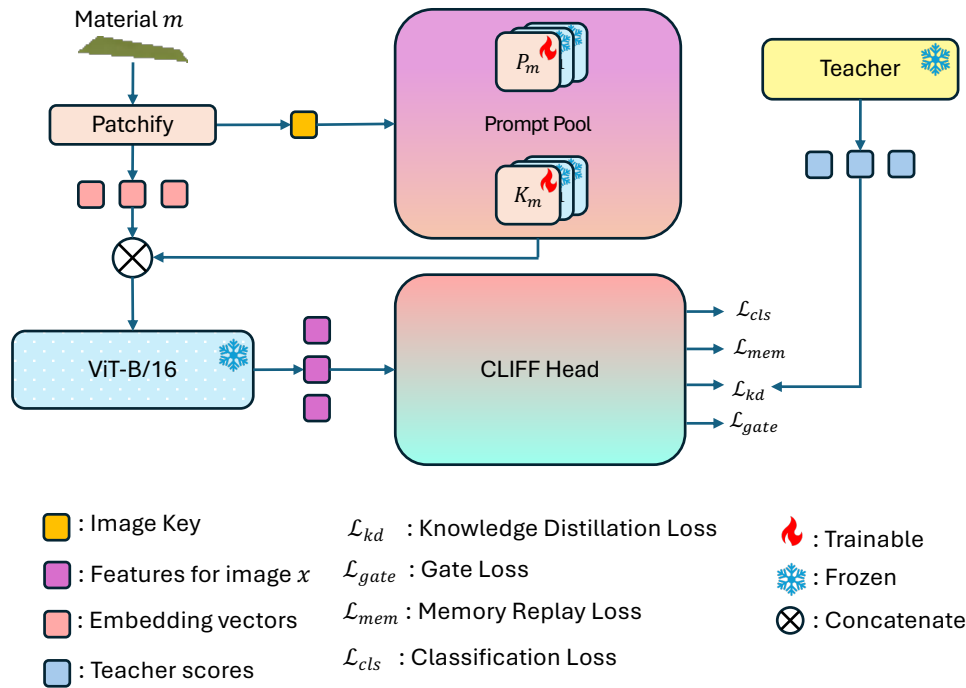


Figure 2: The proposed CLIFF approach.

parameters for new tasks [59, 23] or sub-networks specialized for a certain task, which are maintained [57, 20]. Limitations of this approach include the added complexity of the parameters and the model, and the requirement to specify the task type beforehand, which may not be available at test time. In prompt-based learning [56, 55], the backbone is kept frozen, and the model learns a set of task-specific prompt tokens to guide it on new tasks.

3 The Proposed Method

This work proposes CLIFF, a continual learning framework for 2D flake layer classification. The architecture is visualized in Figure 2. The core idea is to freeze a robust, general-purpose backbone and a base classification head after training on a reference material. For each subsequent material, the framework learns a small set of new components: a dedicated prompt pool, a material embedding, and a delta head that models a material-specific correction. A prompt pool adapts the frozen backbone’s features during training on a new material by prepending learned tokens to the input patch sequence. To further combat catastrophic forgetting, a rehearsal strategy is employed that replays a small number of stored samples from previous tasks. Knowledge distillation is applied to replayed samples, where a static copy of the model from the previous task serves as a “teacher,” ensuring the current model retains prior knowledge. The final classification head computes predictions for all observed materials in parallel, guided by an auxiliary loss term for material identity. This allows the approach to perform task-agnostic classification without needing material labels at test time.

3.1 Base Training on a Reference Material

Let $D_0 = \{(x_i, y_i)\}_{i=1}^{N_0}$ be the reference material dataset, where x_i represents the i -th input image and $y_i \in \{\text{Few}, \text{Mono}, \text{Thick}\}$ is the corresponding thickness label. A Vision Transformer (ViT) [8] backbone f_θ with parameters θ and a linear classification head g_ϕ with parameters ϕ are trained by optimizing the

base loss function shown in Equation (1) as follows,

$$\mathcal{L}_{base} = \frac{1}{N_0} \sum_{i=1}^{N_0} \text{CE}(b(x_i), y_i) = \frac{1}{N_0} \sum_{i=1}^{N_0} \text{CE}(g_\phi(f_\theta(x_i)), y_i), \quad (1)$$

where $\text{CE}(\cdot, \cdot)$ denotes the cross-entropy loss function and $b(x_i) = g_\phi(f_\theta(x_i))$ represents the base classification logits for image x_i .

3.2 Incremental Learning for New Materials

When a new material m arrives, the approach introduces three new learnable components: a prompt P_m , a material embedding e_m , and a delta head D_m .

3.2.1 Prompting

For each material m , the model learns a separate prompt pool P_m . Each is initialized as a new set of learnable parameters, consisting of prompt tokens and their corresponding keys, with values drawn from a random uniform distribution. During training, the model selects a set of these prompt tokens by choosing the top- k tokens with the highest cosine similarity between the mean of the input patch embeddings and the prompt keys. These selected tokens are then prepended to the sequence of image patch embeddings before the frozen transformer backbone processes them. The prompt tokens and their corresponding keys are optimized via backpropagation with respect to the final task loss. This allows for material-specific adaptation of the backbone’s features without altering its weights. The feature output from the prompted backbone is denoted as Equation (2):

$$z_m = f_\theta(x; P_m), \quad (2)$$

where the output feature z_m is now conditioned on the specific prompt pool P_m .

3.2.2 CLIFF Head

The CLIFF head’s architecture is visualized in Figure 3. It processes the prompted features $z_m \in \mathbb{R}^d$, where d is the backbone’s feature dimension. It maintains an embedding table $E \in \mathbb{R}^{M \times d_e}$ containing a unique embedding vector e_i for each of the M seen materials, where d_e is the embedding dimension. At inference, CLIFF evaluates all material-specific delta heads in parallel.

For each material m , the Delta Head is implemented as a multilayer perceptron (MLP) consisting of a linear projection to a hidden dimension of 384, a GELU activation, and a Dropout layer ($p = 0.2$), followed by a final linear projection. It computes a residual correction $\Delta_i(x) \in \mathbb{R}^C$ as described in Equation (3):

$$\Delta_m(x) = D_m(\text{Concat}[z_m, e_m]). \quad (3)$$

Here, $C = 3$ is the number of thickness classes. The final output is a single, large logit vector $L(x)$ created by concatenating the corrected logits for all M materials, as calculated using Equation (4):

$$L(x) = \text{Concat}_{i=1}^M (b(x) + \Delta_i(x)) \in \mathbb{R}^{CM}. \quad (4)$$

The prediction is the argmax over this global CM -dimensional label space.

3.2.3 Optimization with Rehearsal and Distillation

With f_θ and g_ϕ frozen, new components (P_m, e_m, D_m) are learned for a new material. A small memory buffer \mathcal{M} containing samples from past tasks is maintained. The total loss for a sample (x, y) from the current task m is calculated as shown in Equation (5):

$$\mathcal{L} = \mathcal{L}_{cls} + \lambda_{gate} \mathcal{L}_{gate} + \lambda_{mem} \mathcal{L}_{mem} + \lambda_{kd} \mathcal{L}_{kd}. \quad (5)$$

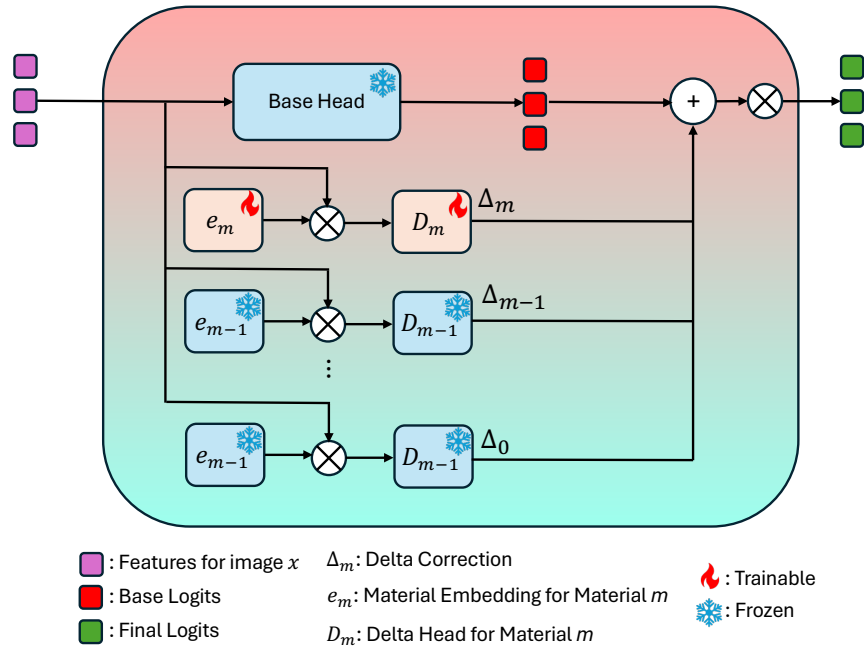


Figure 3: Internal architecture of the CLIFF Head. This illustrates the pipeline for new-image features. Replayed features follow the same process to produce student prediction scores.

Here, \mathcal{L}_{cls} is the standard cross-entropy loss on the current task’s data. The auxiliary gate loss, $\mathcal{L}_{\text{gate}}$, supervises material awareness. The method computes the cosine similarity between the projected feature $q(z)$ and the normalized material embeddings E , scaled by a temperature τ . The similarity is optimized using the cross-entropy against the ground truth material index y_{mat} . This is shown in Equation (6):

$$\mathcal{L}_{\text{gate}} = \text{CE} \left(\text{Softmax} \left(\frac{q(z) \cdot E^T}{\tau} \right), y_{\text{mat}} \right). \quad (6)$$

While the cosine-similarity gate supervises material awareness/prompt selection, it does not mask or disable any heads at inference. \mathcal{L}_{mem} is the cross-entropy loss for samples replayed from the memory buffer \mathcal{M} . Finally, \mathcal{L}_{kd} is a knowledge distillation loss. Kullback-Leibler divergence is used between the logits of the current model (S) and a frozen ”teacher” model (T), which is a snapshot of the model from the previous task. Using a distillation temperature τ_{kd} , the loss is defined as shown in Equation (7):

$$\mathcal{L}_{\text{kd}} = \tau_{\text{kd}}^2 \cdot \text{KL} \left(\sigma \left(\frac{z_S}{\tau_{\text{kd}}} \right) \parallel \sigma \left(\frac{z_T}{\tau_{\text{kd}}} \right) \right), \quad (7)$$

where σ denotes the softmax function. Using knowledge distillation on replayed samples encourages the current model’s outputs to match those from the teacher. The memory buffer \mathcal{M} has a fixed capacity per class. To ensure that the buffer retains a diverse representation of the data distribution over long task sequences, a random replacement strategy is employed. Once the buffer for a class is full, new samples replace existing ones with a probability of 0.1. This stochastic update mechanism prevents the memory from becoming static and allows the buffer to gradually drift towards a representative uniform sample for the aggregate dataset as training progresses. In the experiments shown in Table 1, this is set to 100 samples. In Table 4, the effect of the memory bank is analyzed. During training on task m , the classification loss \mathcal{L}_{cls} is computed over the C -dimensional logits corresponding to material m . The overall training procedure for material m is summarized in Algorithm 1.

3.3 Complexity

The total parameter count grows linearly with the number of materials M , i.e., $\mathcal{O}(M)$, while the backbone parameters remain constant. For each new material, the added parameters comprise prompt to-

Algorithm 1 CLIFF Training Procedure for Material m

Require: Frozen backbone f_θ , Base head g_ϕ , Memory \mathcal{M}
Require: New dataset \mathcal{D}_m , Previous Teacher T (if $m > 0$)

- 1: Initialize prompt pool P_m , embedding e_m , Delta Head D_m
- 2: **for** epoch = 1 to E **do**
- 3: **for** batch (x, y) in \mathcal{D}_m **do**
- 4: // **Forward pass on new data**
- 5: Get features $z = f_\theta(x; P_m)$
- 6: Compute base logits $b = g_\phi(z)$
- 7: Compute correction $\Delta = D_m([z, e_m])$
- 8: Loss $\mathcal{L}_{cls} = \text{CE}(b + \Delta, y)$
- 9: Loss $\mathcal{L}_{gate} = \text{CE}(\text{Sim}(z, E), m)$
- 10: // **Replay Step**
- 11: Sample (x_{mem}, y_{mem}) from \mathcal{M}
- 12: Compute \mathcal{L}_{mem} on student predictions
- 13: **if** $m > 0$ **then**
- 14: Get teacher logits $L_T = T(x_{mem})$
- 15: Compute $\mathcal{L}_{kd} = \text{KL}(L_S || L_T)$
- 16: **end if**
- 17: **Update** P_m, e_m, D_m to minimize \mathcal{L}_{total}
- 18: **end for**
- 19: **end for**
- 20: Update Memory \mathcal{M} with samples from \mathcal{D}_m using random replacement

kens, prompt keys, a material embedding, and a delta head. The approximate per-material parameter count is

$$\underbrace{KLd}_{\text{prompt tokens}} + \underbrace{Kd}_{\text{prompt keys}} + \underbrace{d_e}_{\text{embedding}} + \underbrace{(d+d_e)h + hC}_{\text{delta head}}, \quad (8)$$

where K is the prompt pool size, L is the prompt length, d is the backbone’s feature dimension, d_e is the embedding dimension, h is the delta head’s hidden dimension, and C is the number of classes. The total parameter count scales as $O(M)$. At inference, evaluating all heads incurs an $O(M)$ computational cost per image. For rehearsal, a memory buffer that stores n RGB images per class at a resolution of 224×224 requires approximately $M \cdot C \cdot n \cdot 224^2 \cdot 3$ bytes of storage.

4 Experimental Setup

4.1 Datasets

In this study, the dataset is sourced from Masubuchi et al. [25] and addresses material-incremental layer classification across four materials: BN (base), graphene, MoS₂, and WTe₂. Each image x is labeled as Few, Mono, or Thick with its material type (e.g., Mono_BN). To improve robustness against variations inherent in optical microscopy, augmentations are applied during training. Given an arbitrary orientation of flakes on a substrate, random horizontal ($p = 0.5$) and vertical ($p = 0.3$) flips, as well as random rotations up to 15°, are also applied. Additionally, to simulate varying illumination conditions, further augmentations include color jittering and randomly adjusted brightness, contrast, and saturation by a factor of 0.2. Finally, all images are resized to 224×224 resolution and normalized using the standard ImageNet mean and standard deviation.

4.2 Evaluation Protocol

Training and evaluation are conducted using the following materials in order: BN (T1), graphene (T2), MoS₂ (T3), and WTe₂ (T4). Reported metrics include per-material accuracy at each step, the final macro-average accuracy, and forgetting, the average drop from each material’s peak accuracy to its final accuracy.

Table 1: Sequential task performance on four materials: BN (T1), Graphene (T2), MoS₂ (T3), and WTe₂ (T4). The reported metrics include per-task accuracy, final average accuracy, and forgetting.

	Trained on	Tested on (Accuracy %)			
		T1	T2	T3	T4
Joint Training	Ensemble	92.68	92.04	90.91	92.82
	<i>Summary</i>	Avg. Accuracy: 92.11%			
Naive Fine-tuning	T1	91.46	-	-	-
	T2	10.98	86.09	-	-
	T3	8.54	22.23	83.77	-
	T4	4.88	3.20	0.65	62.68
	<i>Summary</i>	Avg. Accuracy: 17.85%		Forgetting: 84.20%	
L2P [56]	T1	85.37	-	-	-
	T2	60.98	82.34	-	-
	T3	57.32	52.88	87.66	-
	T4	53.66	21.23	1.30	71.77
	<i>Summary</i>	Avg. Accuracy: 36.99%		Forgetting: 59.73%	
CLIFF	T1	90.24	-	-	-
	T2	86.59	79.33	-	-
	T3	64.63	77.70	79.87	-
	T4	56.10	44.79	44.16	82.78
	<i>Summary</i>	Avg. Accuracy: 56.96%		Forgetting: 34.80%	

4.3 Implementation Details

All experiments are performed using a Vision Transformer backbone (ViT-B/16) initialized with DeiT-Base [45] weights. The model is trained for 15 epochs per task with a batch size of 32, using an Adam optimizer with a learning rate of 5×10^{-5} for the delta heads and 1×10^{-4} for the prompts. The Delta Heads are MLPs with a hidden dimension of 384 and a dropout rate of 0.2. The approach utilizes a memory bank of 100 samples per class. The knowledge distillation weight (λ_{kd}) is 1.0 with a temperature $\tau_{kd} = 3.0$, and the gate loss weight is $\lambda_{gate} = 0.1$ with a temperature $\tau = 1.0$. The material embedding dimension is 128, and each per-material prompt pool contains 30 prompts of length 8. The proposed approach is evaluated against three baselines: (1) Joint Training, an upper-bound model trained with data from all four materials simultaneously rather than sequentially; (2) Naive Fine-tuning, a sequential strategy that updates the full model for each new task; and (3) L2P (Learning to Prompt), a prompt-based continual learning method that keeps the backbone frozen while learning a shared pool of prompts for adaptation.

5 Results and Analysis

5.1 Method Comparisons

The Masubuchi et al. dataset [25] labels flakes as monolayers, few-layers, or thick, and Table 1 summarizes the performance of different approaches on this classification task. Joint training serves as an upper bound, achieving strong performance across all tasks. Naive fine-tuning performs well on the most recently trained task but suffers from catastrophic forgetting, with earlier tasks showing severe degradation, resulting in a low final average accuracy and high forgetting. L2P significantly outperforms naive fine-tuning, achieving a higher average accuracy and a reduced, yet still substantial, level of forgetting. In contrast, the proposed method maintains competitive performance on new tasks while substantially preserving accuracy on earlier ones, yielding a significantly higher final average accuracy and lower forgetting than both naive fine-tuning and L2P.



Figure 4: Visual comparison of classification predictions on a `Thick_BN` flake (Task 1) after training on all four tasks. The bounding box indicates the input crop. CLIFF (Green) correctly predicts the label, whereas Naive Fine-tuning and L2P (Red) fail due to catastrophic forgetting.

5.2 Qualitative Analysis

To understand the practical implications for the quantitative results, the model predictions for real-world microscopy contexts are visualized. Figure 4 illustrates a "Thick BN" flake situated within its original microscopy image. After the model has finished training on all four tasks, its ability to classify this specific region is evaluated. Both naive finetuning and L2P fail to recognize the material, misclassifying it as "Thick WTe₂" and "Few MoS₂" respectively. This is likely a consequence of overfitting to the most recent tasks. In contrast, CLIFF correctly classifies the flake, demonstrating the ability to retain material-specific visual features over long training sequences. Further samples are provided in Table 2, which details specific predictions for various flake crops. Similarly, the baselines exhibit a bias towards the most recent tasks and mislabel earlier samples.

5.3 Ablation Studies

The ablation experiments study the contribution of each key component and its configurations. The removal of primary components is explored in Table 3 to investigate their contributions. The removal of

Table 2: Qualitative comparison of predictions on specific flake samples. The comparisons include Naive Fine-tuning (FT), L2P, and CLIFF against the Ground Truth (GT). CLIFF consistently predicts the correct label even for older tasks (BN, Graphene), whereas baselines often misclassify labels from the most recent tasks (WTe₂).

Input (GT)	Naive FT	L2P	CLIFF
 <i>Thick BN</i>	Thick WTe ₂ ✗	Few MoS ₂ ✗	Thick BN ✓
 <i>Mono Graphene</i>	Mono WTe ₂ ✗	Few MoS ₂ ✗	Mono Graphene ✓
 <i>Few MoS₂</i>	Thick WTe ₂ ✗	Few MoS ₂ ✓	Few MoS ₂ ✓
 <i>Few WTe₂</i>	Few WTe ₂ ✓	Thick Graphene ✗	Few WTe ₂ ✓

Table 3: Effectiveness of CLIFF on the material-incremental benchmark with different configurations.

Memory	KD	Prompts	Avg. Acc. (%)	Forgetting (%)
		✓	18.80	79.64
✓	✓		57.44	32.78
✓	✓	✓	56.95	34.80

memory replay and knowledge distillation results in a massive drop in performance, showing that rehearsal is the core mechanism for retaining knowledge. Removing only prompts results in slightly lower forgetting and higher average accuracy. This result reveals a plasticity-stability trade-off, where prompts allow higher peak accuracy on new tasks (e.g., 79.87% on Task 3 vs. 75.97% without prompts). At the same time, the CLIFF Head provides strong underlying stability, resulting in slightly lower overall forgetting when it operates alone. Additionally, the impact of the memory buffer size is quantitatively shown by Table 4. Performance degrades as the buffer shrinks, but even a small memory of 20 samples per class provides a substantial benefit over having no memory at all.

Table 4: Impact of memory buffer size on final average accuracy and forgetting.

Mem. Size	Avg. Acc. (%)	Forgetting (%)
0	18.80	79.64
20	31.47	56.12
40	35.95	53.12
60	42.56	46.38
80	49.85	37.64
100	56.95	34.80

6 Conclusion

This paper has introduced CLIFF, a continual learning framework for 2D material layer classification that adapts to new materials by learning material-specific information while retaining prior knowledge through memory rehearsal with knowledge distillation. The strong performance of CLIFF makes it a valuable tool for practical laboratory use. It is well-suited to accelerate the identification of promising flakes across different materials, significantly reducing the manual effort required for expert verification. The experiments have demonstrated that CLIFF substantially improves average accuracy and reduces forgetting compared to naive fine-tuning and a strong prompt-based baseline. This work has presented the first systematic study of continual learning for this problem, bridging the gap between current deep learning models and the practical needs of real-world laboratories.

6.1 Limitations

Although CLIFF significantly reduces catastrophic forgetting and improves the applicability of continual learning for real-world materials science, a concern with this architecture is scalability. CLIFF adds new parameters for each new material and computes corrections for all seen materials at inference time. While this is feasible within the current scope of this work, linear growth in the number of parameters could lead to heavy computation across hundreds of materials. Additionally, performance depends on the memory buffer, which introduces storage overhead and assumes replayed samples are sufficient to account for feature-space shifts. Future work could investigate parameter-sharing techniques to address scalability, explicit feature alignment to handle feature space shifts, and knowledge transfer between optically similar materials to reduce data dependency.

6.2 Broader Impacts

CLIFF improves the practicality and usability of automated quantum flake characterization. By enabling deep learning models to adapt to new materials efficiently without forgetting old knowledge, this ap-

proach accelerates the pace of discovery in 2D material analysis. It promotes the broader application of robust AI systems in scientific research.

Acknowledgments

This work is partly supported by MonArk NSF Quantum Foundry (DMR-1906383) and NSF Quantum Award (2444042). It acknowledges the Arkansas High-Performance Computing Center for providing GPUs.

References

- [1] A. F. Agarap. Deep learning using rectified linear units (relu). *arXiv preprint arXiv:1803.08375*, 2018.
- [2] P. Buzzega, M. Boschini, A. Porrello, D. Abati, and S. Calderara. Dark experience for general continual learning: a strong, simple baseline, 2020.
- [3] H. Cha, J. Lee, and J. Shin. Co²l: Contrastive continual learning, 2021.
- [4] A. Chaudhry, A. Gordo, P. K. Dokania, P. Torr, and D. Lopez-Paz. Using hindsight to anchor past knowledge in continual learning, 2021.
- [5] A. Chaudhry, M. Ranzato, M. Rohrbach, and M. Elhoseiny. Efficient lifelong learning with a-gem, 2019.
- [6] A. Chaudhry, M. Rohrbach, M. Elhoseiny, T. Ajanthan, P. K. Dokania, P. H. S. Torr, and M. Ranzato. On tiny episodic memories in continual learning, 2019.
- [7] A. Dendukuri, B. Keeling, A. Fereidouni, J. Burbridge, K. Luu, and H. Churchill. Defining quantum neural networks via quantum time evolution. *arXiv preprint arXiv:1905.10912*, 2019.
- [8] A. Dosovitskiy, L. Beyer, A. Kolesnikov, D. Weissenborn, X. Zhai, T. Unterthiner, M. Dehghani, M. Minderer, G. Heigold, S. Gelly, J. Uszkoreit, and N. Houlsby. An image is worth 16x16 words: Transformers for image recognition at scale, 2021.
- [9] E. Fix and J. L. Hodges. Discriminatory analysis. nonparametric discrimination: Consistency properties. *International Statistical Review / Revue Internationale de Statistique*, 57(3):238–247, 1989.
- [10] B. Han, Y. Lin, Y. Yang, N. Mao, W. Li, H. Wang, K. Yasuda, X. Wang, V. Fatemi, L. Zhou, et al. Deep-learning-enabled fast optical identification and characterization of 2d materials. *Advanced Materials*, 32(29):2000953, 2020.
- [11] T. L. Hayes, N. D. Cahill, and C. Kanan. Memory efficient experience replay for streaming learning, 2019.
- [12] K. He, G. Gkioxari, P. Dollár, and R. Girshick. Mask r-cnn. In *Proceedings of the IEEE international conference on computer vision*, pages 2961–2969, 2017.
- [13] M. A. Hearst, S. T. Dumais, E. Osuna, J. Platt, and B. Scholkopf. Support vector machines. *IEEE Intelligent Systems and their applications*, 13(4):18–28, 1998.
- [14] J. B. Holliday, D. Blount, H. Q. Nguyen, S. U. Khan, and K. Luu. Quadro: A hybrid quantum optimization framework for drone delivery. In *2025 IEEE International Conference on Quantum Computing and Engineering (QCE)*, volume 01, pages 2090–2100, 2025.
- [15] J. B. Holliday, D. Blount, E. Osaba, and K. Luu. Advanced quantum annealing approach to vehicle routing problems with time windows, 2025.

- [16] J. B. Holliday, B. Morgan, H. Churchill, and K. Luu. Hybrid quantum tabu search for solving the vehicle routing problem. In *2024 IEEE international conference on quantum computing and engineering (QCE)*, volume 2, pages 353–358. IEEE, 2024.
- [17] J. B. Holliday, E. Osaba, and K. Luu. An advanced hybrid quantum tabu search approach to vehicle routing problems, 2025.
- [18] S. Ioffe and C. Szegedy. Batch normalization: Accelerating deep network training by reducing internal covariate shift. In *International conference on machine learning*, pages 448–456. pmlr, 2015.
- [19] K. James Singh, T. Ahmed, P. Gautam, A. S. Sadhu, D.-H. Lien, S.-C. Chen, Y.-L. Chueh, and H.-C. Kuo. Recent advances in two-dimensional quantum dots and their applications. *Nanomaterials*, 11(6):1549, 2021.
- [20] Z. Ke, B. Liu, and X. Huang. Continual learning of a mixed sequence of similar and dissimilar tasks, 2021.
- [21] A. Kirillov, E. Mintun, N. Ravi, H. Mao, C. Rolland, L. Gustafson, T. Xiao, S. Whitehead, A. C. Berg, W.-Y. Lo, et al. Segment anything. In *Proceedings of the IEEE/CVF international conference on computer vision*, pages 4015–4026, 2023.
- [22] M. C. Lemme, D. Akinwande, C. Huyghebaert, and C. Stampfer. 2d materials for future heterogeneous electronics. *Nature communications*, 13(1):1392, 2022.
- [23] X. Li, Y. Zhou, T. Wu, R. Socher, and C. Xiong. Learn to grow: A continual structure learning framework for overcoming catastrophic forgetting, 2019.
- [24] J. Liu, Y. Ding, M. Zeng, and L. Fu. Chemical insights into two-dimensional quantum materials. *Matter*, 5(7):2168–2189, 2022.
- [25] S. Masubuchi, E. Watanabe, Y. Seo, S. Okazaki, T. Sasagawa, K. Watanabe, T. Taniguchi, and T. Machida. Deep-learning-based image segmentation integrated with optical microscopy for automatically searching for two-dimensional materials. *npj 2D Materials and Applications*, 4(1):3, 2020.
- [26] H.-Q. Nguyen, X. B. Nguyen, S. Y.-C. Chen, H. Churchill, N. Borys, S. U. Khan, and K. Luu. Diffusion-inspired quantum noise mitigation in parameterized quantum circuits. *Quantum Machine Intelligence*, 7(1):55, 2025.
- [27] H.-Q. Nguyen, X.-B. Nguyen, H. Churchill, A. K. Choudhary, P. Sinha, S. U. Khan, and K. Luu. Quantum-brain: Quantum-inspired neural network approach to vision-brain understanding, 2025.
- [28] H.-Q. Nguyen, X. B. Nguyen, S. Pandey, T. Faltermeier, N. Borys, H. Churchill, and K. Luu. φ -adapt: A physics-informed adaptation learning approach to 2d quantum material discovery, 2025.
- [29] H.-Q. Nguyen, X.-B. Nguyen, S. Pandey, S. U. Khan, I. Safro, and K. Luu. Qmoe: A quantum mixture of experts framework for scalable quantum neural networks. In *2025 IEEE International Conference on Quantum Computing and Engineering (QCE)*, volume 02, pages 223–228, 2025.
- [30] P. Nguyen, T.-D. Truong, M. Huang, Y. Liang, N. Le, and K. Luu. Self-supervised domain adaptation in crowd counting. In *2022 IEEE international conference on image processing (ICIP)*, pages 2786–2790. IEEE, 2022.
- [31] P. Nguyen, T.-D. Truong, M. Huang, Y. Liang, N. Le, and K. Luu. Self-supervised domain adaptation in crowd counting. In *2022 IEEE International Conference on Image Processing (ICIP)*, pages 2786–2790, 2022.
- [32] X. B. Nguyen, A. Bisht, B. Thompson, H. Churchill, K. Luu, and S. U. Khan. Two-dimensional quantum material identification via self-attention and soft-labeling in deep learning. *IEEE Access*, 2024.

- [33] X. B. Nguyen, H. Churchill, K. Luu, and S. U. Khan. Quantum vision clustering. *arXiv preprint arXiv:2309.09907*, 2023.
- [34] X.-B. Nguyen, G.-S. Lee, S.-H. Kim, and H.-J. Yang. Audio-video based emotion recognition using minimum cost flow algorithm. In *2019 IEEE/CVF International Conference on Computer Vision Workshop (ICCVW)*, pages 3737–3741, 2019.
- [35] X.-B. Nguyen, H.-Q. Nguyen, S. Y.-C. Chen, S. U. Khan, H. Churchill, and K. Luu. Qclusformer: A quantum transformer-based framework for unsupervised visual clustering, 2024.
- [36] X.-B. Nguyen, H.-Q. Nguyen, H. Churchill, S. U. Khan, and K. Luu. Hierarchical quantum control gates for functional mri understanding. In *2024 IEEE Workshop on Signal Processing Systems (SiPS)*, pages 159–164. IEEE, 2024.
- [37] X.-B. Nguyen, H.-Q. Nguyen, H. Churchill, S. U. Khan, and K. Luu. Quantum visual feature encoding revisited. *Quantum Machine Intelligence*, 6(2):61, 2024.
- [38] X.-B. Nguyen, M. Serna-Aguilera, A. K. Choudhary, P. Sinha, X. Li, and K. Luu. Cobra: A continual learning approach to vision-brain understanding: Cobra: A continual learning approach... *Int. J. Comput. Vision*, 134(1), Jan. 2026.
- [39] X.-B. Nguyen, T.-D. Truong, P. Sinha, and K. Luu. Brain: Bias-mitigation continual learning approach to vision-brain understanding, 2025.
- [40] Q. Pham, C. Liu, and S. Hoi. Dualnet: Continual learning, fast and slow, 2021.
- [41] N. Ravi, V. Gabeur, Y.-T. Hu, R. Hu, C. Ryali, T. Ma, H. Khedr, R. Rädle, C. Rolland, L. Gustafson, et al. Sam 2: Segment anything in images and videos. *arXiv preprint arXiv:2408.00714*, 2024.
- [42] S.-A. Rebuffi, A. Kolesnikov, G. Sperl, and C. H. Lampert. icarl: Incremental classifier and representation learning, 2017.
- [43] O. Ronneberger, P. Fischer, and T. Brox. U-net: Convolutional networks for biomedical image segmentation. In *Medical image computing and computer-assisted intervention–MICCAI 2015: 18th international conference, Munich, Germany, October 5-9, 2015, proceedings, part III 18*, pages 234–241. Springer, 2015.
- [44] R. Shokri and V. Shmatikov. Privacy-preserving deep learning. In *2015 53rd Annual Allerton Conference on Communication, Control, and Computing (Allerton)*, pages 909–910, 2015.
- [45] H. Touvron, M. Cord, M. Douze, F. Massa, A. Sablayrolles, and H. Jegou. Training data-efficient image transformers & distillation through attention. In *International Conference on Machine Learning*, volume 139, pages 10347–10357, July 2021.
- [46] T.-D. Truong, R. T. N. Chappa, X.-B. Nguyen, N. Le, A. P. Dowling, and K. Luu. OTAdapt: Optimal Transport-based Approach For Unsupervised Domain Adaptation . In *2022 26th International Conference on Pattern Recognition (ICPR)*, pages 2850–2856, Los Alamitos, CA, USA, Aug. 2022. IEEE Computer Society.
- [47] T.-D. Truong, C. N. Duong, P. Helton, A. Dowling, X. Li, and K. Luu. Comal: Conditional maximum likelihood approach to self-supervised domain adaptation in long-tail semantic segmentation. *arXiv preprint arXiv:2304.07372*, 2023.
- [48] T.-D. Truong, C. N. Duong, N. Le, S. L. Phung, C. Rainwater, and K. Luu. Bimal: Bijective maximum likelihood approach to domain adaptation in semantic scene segmentation. In *Proceedings of the IEEE/CVF International Conference on Computer Vision*, pages 8548–8557, 2021.

- [49] T.-D. Truong, C. N. Duong, N. Le, S. L. Phung, C. Rainwater, and K. Luu. Bimal: Bijective maximum likelihood approach to domain adaptation in semantic scene segmentation. In *2021 IEEE/CVF International Conference on Computer Vision (ICCV)*, pages 8528–8537, 2021.
- [50] T.-D. Truong, P. Helton, A. Moustafa, J. D. Cothren, and K. Luu. Conda: Continual unsupervised domain adaptation learning in visual perception for self-driving cars. In *Proceedings of the IEEE/CVF Conference on Computer Vision and Pattern Recognition (CVPR) Workshops*, pages 5642–5650, June 2024.
- [51] T.-D. Truong, N. Le, B. Raj, J. Cothren, and K. Luu. Freedom: Fairness domain adaptation approach to semantic scene understanding. In *Proceedings of the IEEE/CVF conference on computer vision and pattern recognition*, pages 19988–19997, 2023.
- [52] T.-D. Truong, H.-Q. Nguyen, B. Raj, and K. Luu. Fairness continual learning approach to semantic scene understanding in open-world environments. *Advances in Neural Information Processing Systems*, 36:65456–65467, 2023.
- [53] T.-D. Truong, U. Prabhu, B. Raj, J. Cothren, and K. Luu. Falcon: Fairness learning via contrastive attention approach to continual semantic scene understanding. In *The IEEE/CVF Conference on Computer Vision and Pattern Recognition*, 2025.
- [54] J.-L. Uslu, T. Ouaj, D. Tebbe, A. Nekrasov, J. H. Bertram, M. Schütte, K. Watanabe, T. Taniguchi, B. Beschoten, L. Waldecker, et al. An open-source robust machine learning platform for real-time detection and classification of 2d material flakes. *Machine Learning: Science and Technology*, 5(1):015027, 2024.
- [55] Z. Wang, Z. Zhang, S. Ebrahimi, R. Sun, H. Zhang, C.-Y. Lee, X. Ren, G. Su, V. Perot, J. Dy, and T. Pfister. Dualprompt: Complementary prompting for rehearsal-free continual learning, 2022.
- [56] Z. Wang, Z. Zhang, C.-Y. Lee, H. Zhang, R. Sun, X. Ren, G. Su, V. Perot, J. Dy, and T. Pfister. Learning to prompt for continual learning, 2022.
- [57] M. Wortsman, V. Ramanujan, R. Liu, A. Kembhavi, M. Rastegari, J. Yosinski, and A. Farhadi. Supermasks in superposition, 2020.
- [58] Y. Wu, Y. Chen, L. Wang, Y. Ye, Z. Liu, Y. Guo, and Y. Fu. Large scale incremental learning, 2019.
- [59] T. Zhao, Z. Wang, A. Masoomi, and J. Dy. Deep bayesian unsupervised lifelong learning, 2021.